

# Smart Inverter Grid Probing for Learning Loads: Part II – Probing Injection Design

Siddharth Bhela, *Student Member, IEEE*, Vassilis Kekatos, *Senior Member, IEEE*, and Sriharsha Veeramachaneni

**Abstract**—This two-part work puts forth the idea of engaging power electronics to probe an electric grid to infer non-metered loads. Probing can be accomplished by commanding inverters to perturb their power injections and record the induced voltage response. Once a probing setup is deemed topologically observable by the tests of Part I, Part II provides a methodology for designing probing injections abiding by inverter and network constraints to improve load estimates. The task is challenging since system estimates depend on both probing injections and unknown loads in an implicit nonlinear fashion. The methodology first constructs a library of candidate probing vectors by sampling over the feasible set of inverter injections. Leveraging a linearized grid model and a robust approach, the candidate probing vectors violating voltage constraints for any anticipated load value are subsequently rejected. Among the qualified candidates, the design finally identifies the probing vectors yielding the most diverse system states. The probing task under noisy phasor and non-phasor data is tackled using a semidefinite-program (SDP) relaxation. Numerical tests using synthetic and real-world data on a benchmark feeder validate the conditions of Part I; the SDP-based solver; the importance of probing design; and the effects of probing duration and noise.

**Index Terms**—Smart inverters, power system state estimation, Farka’s lemma, max-sum diversity, semi-definite relaxation.

## I. INTRODUCTION

Part I of this work put forth the novel data acquisition scheme of probing-to-learn (P2L). The P2L scheme leverages smart inverters to probe an electric grid with the purpose of finding the values of non-metered loads. It also provided conditions under which a particular probing setup is successful. In particular, it was shown that given the feeder graph  $\mathcal{G}$ , the locations of non-metered buses  $\mathcal{O}$  and probing buses  $\mathcal{M}$ , and the number of probing actions  $T$ , a simple linear program could tell whether non-metered loads could be recovered or not. Assuming noiseless data, this test relied on the generic rank of the Jacobian matrix  $\mathbf{J}(\{\mathbf{v}_t\})$  related to the P2L equations. It is thus a *topological* rather than a *numerical observability* guarantee [1, Ch. 4.6].

Even for the standard power flow (PF) and power system state estimation (PSSE) setups, topological observability relates to the sparsity structure of the associated Jacobian matrix. This structure alone however cannot adequately capture the numerical column rank of the Jacobian matrix. There exist specification or measurement sets whose Jacobian is full column-rank in general, but becomes ill-conditioned or even singular under specific state values (including the boundaries for voltage collapse); see e.g., [1, Ch. 10], [2]. In addition, once a probing setup is deemed topologically observable, the power injections of probing inverters could be judiciously selected to improve load or state estimates. This is challenging since P2L is an implicit nonlinear identification task, and

probing injections should be comply to network constraints without knowing the non-metered loads.

The contribution of Part II is on two practical aspects of grid probing. First, a systematic approach to design probing injections that conform to grid safety and improve numerical accuracy is developed in Section II. Second, the proposed P2L task is tackled through semidefinite program (SDP)-based solvers presented in Section III. The conditions of Part I along with the probing design process and the solver of Part II, are numerically validated using actual residential load data from the Pecan Street project on the IEEE 34-bus benchmark feeder in Section IV. Conclusions and current research efforts are outlined in Section V.

Adding to the notational conventions of Part I, here the symbol  $\mathbf{1}$  denotes the all-one vector and  $\mathbf{e}_k$  is the  $k$ -th canonical vector; their dimensions would be clear from the context. The notation  $\mathbf{V} \succeq \mathbf{0}$  means that  $\mathbf{V}$  is a Hermitian (complex and conjugate symmetric) positive semidefinite matrix; the matrix trace is denoted by  $\text{Tr}(\cdot)$ ; and  $\|\mathbf{a}\|_2$  is the  $\ell_2$ -norm of vector  $\mathbf{a}$ . The notation  $k = 1 : K$  is a shorthand to  $k = 1, \dots, K$ .

## II. DESIGNING PROBING INJECTIONS

Assuming a probing setup has been deemed successful for a specific  $T$  under the tests of Part I, this section deals with the design of inverter injections. To facilitate the exposition, let us stack the power injections at all probing buses  $\{(p_n, q_n)\}_{n \in \mathcal{M}}$  in vectors  $\mathbf{p}_{\mathcal{M}}$ ,  $\mathbf{q}_{\mathcal{M}}$ , and  $\mathbf{s}_{\mathcal{M}} := [\mathbf{p}_{\mathcal{M}}^T \ \mathbf{q}_{\mathcal{M}}^T]^T$ . The injections at probing time  $t$  will be indexed by  $t$  as a superscript. Likewise, the injections at all non-metered buses  $\{(p_n, q_n)\}_{n \in \mathcal{O}}$  are collected in  $\mathbf{p}_{\mathcal{O}}$ ,  $\mathbf{q}_{\mathcal{O}}$ , and  $\mathbf{s}_{\mathcal{O}} := [\mathbf{p}_{\mathcal{O}}^T \ \mathbf{q}_{\mathcal{O}}^T]^T$ .

In search of a meaningful metric to design the probing injections  $\{\mathbf{s}_{\mathcal{M}}^t\}_{t=1}^T$ , one could consider the minimum mean square estimation error for non-metered loads  $\mathbf{s}_{\mathcal{O}}$  or states  $\{\mathbf{v}_t\}_{t=1}^T$ . The former is hard to derive given the implicit estimation task involved. The latter exhibits the Cramer-Rao lower bound (CRLB) of  $[\mathbf{J}^T(\{\mathbf{v}_t\})\mathbf{J}(\{\mathbf{v}_t\})]^{-1}$ ; a proof for this CRLB can be obtained by adopting the result in [3]. Since  $\mathbf{J}(\{\mathbf{v}_t\})$  depends linearly on  $\{\mathbf{v}_t\}_{t=1}^T$ , the CRLB depends inverse quadratically on the unknown states.

To arrive at a practical solution, we resort to selecting probing injections so that the electric grid is driven to the most diverse states  $\{\mathbf{v}_t\}_{t=1}^T$  while abiding by inverter and feeder operational constraints. We conjecture that probing the grid to effect larger state variations across  $\mathcal{T}$  would yield smaller condition numbers for  $\mathbf{J}(\{\mathbf{v}_t\})$  and  $\mathbf{J}^T(\{\mathbf{v}_t\})\mathbf{J}(\{\mathbf{v}_t\})$ .

Hence, the goal is to design  $\{\mathbf{s}_{\mathcal{M}}^t\}_{t=1}^T$  that yield the most diverse system states  $\{\mathbf{v}_t\}_{t=1}^T$ . Since the system states depend on both  $\{\mathbf{s}_{\mathcal{M}}^t\}_{t=1}^T$  and the unknown  $\mathbf{s}_{\mathcal{O}}$  in a non-linear fashion,

our design adopts a linearized power flow model. The latter can be obtained by taking the first-order Taylor's series approximation of the PF equations with respect to nodal voltages expressed in polar coordinates [4], [5]. Unless a reference system state is available, the linearization occurs at the flat voltage profile of  $\tilde{\mathbf{v}} = v_0\mathbf{1} + j\mathbf{0}$ , and yields the so termed *linearized distribution flow* (LDF) model [6], [5], which can be rearranged for our analysis as

$$\mathbf{y} := \begin{bmatrix} \mathbf{u} - v_0\mathbf{1} \\ \boldsymbol{\theta} \end{bmatrix} = \begin{bmatrix} \mathbf{K} & \mathbf{L} \\ \mathbf{M} & \mathbf{N} \end{bmatrix} \begin{bmatrix} \mathbf{s}_{\mathcal{M}} \\ \mathbf{s}_{\mathcal{O}} \end{bmatrix} \quad (1)$$

where  $\mathbf{u}$  and  $\boldsymbol{\theta}$  collect the voltage magnitudes and angles at all buses excluding the substation; and matrices  $(\mathbf{K}, \mathbf{L}, \mathbf{M}, \mathbf{N})$  depend on the bus admittance matrix  $\mathbf{Y}$ ; see [5], [7]. Armed with a linear mapping between power injections and voltages, the design of  $\{\mathbf{s}_{\mathcal{M}}^t\}_{t=1}^T$  is accomplished next in three steps.

#### A. Build library of implementable probing injections

The first step of the probing design process builds a library  $\mathcal{S}$  of  $K \gg T$  candidate injection vectors indexed by  $k$

$$\mathcal{S} := \{\mathbf{s}_{\mathcal{M}}^k\}_{k=1}^K. \quad (2)$$

The entries of each  $\mathbf{s}_{\mathcal{M}}^k$  should be *implementable*, in the sense that each probing inverter should be able to inject the requested values of (re)active power.

To characterize the allowable range of inverter injections  $(p_n, q_n)$  with  $n \in \mathcal{M}$ , two inverter classes are identified. The first class consists of inverters interfacing solar panels. When inverter  $n$  interfaces a solar panel, its complex injection is limited by its apparent power capacity  $\bar{s}_n$  as

$$p_n^2 + q_n^2 \leq \bar{s}_n^2. \quad (3)$$

Moreover, if the maximum active power that can be generated given the solar irradiance at the current probing period is  $\bar{p}_n$ , then its active power injection is limited by

$$0 \leq p_n \leq \bar{p}_n. \quad (4)$$

The second class consists of inverters interfacing energy storage units. The apparent power constraint of (3) should still be enforced. If the power rate of energy storage unit  $n$  is  $\bar{p}_n$ , the active injection from inverter  $n$  should lie within

$$-\bar{p}_n \leq p_n \leq \bar{p}_n \quad (5)$$

since the battery can be charged or discharged. Given the short duration of probing, state of charge limits are ignored.

Given the limitations for each inverter class, a candidate probing injection  $\mathbf{s}_{\mathcal{M}}^k \in \mathcal{S}$  can be constructed by sampling uniformly at random  $p_n^k$  within (4)–(5) for all  $n \in \mathcal{M}$ . Upon fixing active injections, the reactive injections can be sampled again uniformly at random within  $|q_n^k| \leq \sqrt{\bar{s}_n^2 - (p_n^k)^2}$  to comply with (3). Scenarios where a single bus hosts multiple inverters belonging to the previous two or additional classes can be incorporated in the sampling process.

The sampling process is repeated  $K$  times to construct library  $\mathcal{S}$ . Although each candidate probing vector  $\mathbf{s}_{\mathcal{M}}^k \in \mathcal{S}$  can be implemented by inverters, the aggregate effect of probing injections may be violating feeder constraints. To handle this concern, we next reduce library  $\mathcal{S}$  to only those probing injections abiding by feeder constraints.

#### B. Reduce library to network-compliant probing injections

Event though a probing action lasts for one second, the operator may still want to guarantee that it does not violate any feeder constraints. For example, voltage regulation standards dictate voltage magnitudes to remain within a pre-specified range as  $\underline{v} \leq v_n \leq \bar{v}$  for all  $n \in \mathcal{N}^+$ . A probing injection vector  $\mathbf{s}_{\mathcal{M}}^k \in \mathcal{S}$  is deemed *network-compliant* if the incurred voltage magnitudes are maintained within the allowable range  $\underline{v}\mathbf{1} \leq \mathbf{u} \leq \bar{v}\mathbf{1}$  with the inequalities applied entry-wise. Thanks to (1), these voltage constraints can be alternatively expressed as the linear inequalities

$$\underline{v}\mathbf{1} \leq \mathbf{K}\mathbf{s}_{\mathcal{M}}^k + \mathbf{L}\mathbf{s}_{\mathcal{O}} + v_0\mathbf{1} \leq \bar{v}\mathbf{1}. \quad (6)$$

One cannot directly check whether  $\mathbf{s}_{\mathcal{M}}^k$  is network-compliant, since  $\mathbf{s}_{\mathcal{O}}$  is unknown. To bypass this complication, non-metered loads are assumed to lie within a known range

$$\underline{\mathbf{s}}_{\mathcal{O}} \leq \mathbf{s}_{\mathcal{O}} \leq \bar{\mathbf{s}}_{\mathcal{O}}. \quad (7)$$

The bounds  $(\underline{\mathbf{s}}_{\mathcal{O}}, \bar{\mathbf{s}}_{\mathcal{O}})$  can be derived from historical data, the confidence intervals of load forecasts, or the load estimates obtained during the previous probing period.

Adopting a robust design, we would like to comply with the voltage constraints in (6) for all possible values of non-metered loads in (7). To do so, we leverage the next version of Farka's lemma on the containment of polytopes.

**Lemma 1** ([8], [9], [10]). *The non-empty polytope  $\mathcal{P}_1 := \{\mathbf{x} : \mathbf{A}\mathbf{x} \leq \mathbf{b}\}$  with  $\mathbf{A} \in \mathbb{R}^{M \times N}$  is contained within the polytope  $\mathcal{P}_2 := \{\mathbf{x} : \mathbf{C}\mathbf{x} \leq \mathbf{d}\}$  with  $\mathbf{C} \in \mathbb{R}^{K \times N}$  if and only if there exists matrix  $\mathbf{E} \geq \mathbf{0}$  satisfying  $\mathbf{E}\mathbf{A} = \mathbf{C}$  and  $\mathbf{E}\mathbf{b} \leq \mathbf{d}$ .*

Based on Lemma 1, to ensure that the polytope over  $\mathbf{s}_{\mathcal{O}}$  defined in (7) is contained within the polytope of (6), we need to solve the feasibility problem

$$\begin{aligned} \text{find } & \mathbf{E} \\ \text{s.to } & \mathbf{E} \geq \mathbf{0} \end{aligned} \quad (8)$$

$$\begin{aligned} \mathbf{E} \begin{bmatrix} -\mathbf{I}_{2\mathcal{O}} \\ \mathbf{I}_{2\mathcal{O}} \end{bmatrix} &= \begin{bmatrix} -\mathbf{L} \\ \mathbf{L} \end{bmatrix} \\ \mathbf{E} \begin{bmatrix} -\underline{\mathbf{s}}_{\mathcal{O}} \\ \bar{\mathbf{s}}_{\mathcal{O}} \end{bmatrix} &\leq \begin{bmatrix} \mathbf{K}\mathbf{s}_{\mathcal{M}}^k + (v_0 - \underline{v})\mathbf{1} \\ -\mathbf{K}\mathbf{s}_{\mathcal{M}}^k - (v_0 - \bar{v})\mathbf{1} \end{bmatrix}. \end{aligned}$$

Given  $\mathbf{s}_{\mathcal{M}}^k$ , if the linear program in (8) is feasible, the candidate vector  $\mathbf{s}_{\mathcal{M}}^k$  is deemed network-compliant and is copied to the *reduced library*  $\mathcal{S}_r$ . Otherwise, the candidate vector is not copied to  $\mathcal{S}_r$  since there exist load values within  $[\underline{\mathbf{s}}_{\mathcal{O}}, \bar{\mathbf{s}}_{\mathcal{O}}]$  that violate the voltage constraints in (6). The test of (8) is repeated for all  $\mathbf{s}_{\mathcal{M}}^k \in \mathcal{S}$  to get the reduced library  $\mathcal{S}_r := \{\mathbf{s}_{\mathcal{M}}^{\ell}\}_{\ell=1}^L$  of  $L$  candidate injection vectors with  $L \leq K$ .

To demonstrate the importance of this library reduction step, we ran a numerical test on the IEEE 34-bus feeder for  $T = 4$  and  $O = 10$ ; see Fig. 1. Load uncertainty was confined within a factor of  $\pm\frac{1}{\gamma}$  times the nominal load. The candidate inverter injections in  $\mathcal{S}$  were randomly drawn from  $\pm 0.2$  pu and tested against (8). For increasing  $\gamma$ , the uncertainty bounds in (7) became tighter and progressively more candidate vectors were rendered admissible. Even for loose voltage regulation limits of  $\pm 10\%$  and tight load uncertainty, more than 20% of the candidates in  $\mathcal{S}$  violated (6).

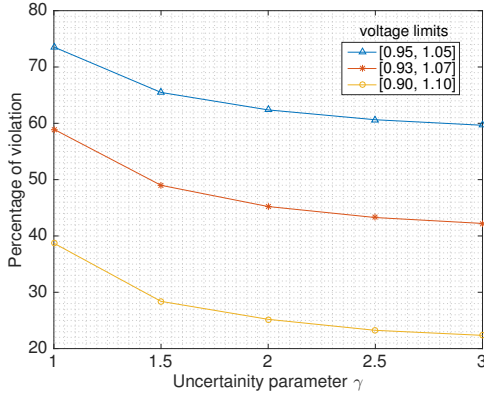


Fig. 1. Percentage of candidate vectors  $\mathbf{s}_{\mathcal{M}}^k \in \mathcal{S}$  that violate (6) for varying voltage bounds  $(\underline{v}, \bar{v})$ . The percentage of non-admissible vectors decreases with smaller load uncertainty and/or looser voltage regulation bounds.

The reduction from  $\mathcal{S}$  to  $\mathcal{S}_r$  via (8) can be generalized. For example, limits on line and transformer flows can be expressed as linear functions of power injections and appended to (6). Moreover, correlations in load forecasts across buses, or power factor limitations applied on a per-bus basis, both can be directly captured as linear inequalities and appended to (7). Finally, if the library reduced significantly so that  $L < T$ , the operator could broaden the voltage regulation interval  $[\underline{v}, \bar{v}]$  and/or tighten the load uncertainty range in (6) if grid probing is still needed to recover non-metered loads.

### C. Find $T$ probing injections with most diverse states

Given the reduced library  $\mathcal{S}_r = \{\mathbf{s}_{\mathcal{M}}^\ell\}_{\ell=1}^L$  of implementable and network-compliant candidates, the last step is to select the  $T$  candidates yielding the most diverse states. Recall that the system state  $\mathbf{v}^\ell$  related to probing injection  $\mathbf{s}_{\mathcal{M}}^\ell$  depends also on the unknown loads  $\mathbf{s}_{\mathcal{O}}$ . Moreover, the dependence on both  $\mathbf{s}_{\mathcal{M}}^\ell$  and  $\mathbf{s}_{\mathcal{O}}$  is non-linear and implicit. The approximate LDF model of (1) can help us circumvent these technical challenges.

The Euclidean distance between the system states induced by injections  $\mathbf{s}_{\mathcal{M}}^\ell, \mathbf{s}_{\mathcal{M}}^{\ell'} \in \mathcal{S}_r$  will be surrogated by the Euclidean distance between the approximate states of (1) as

$$\|\mathbf{v}^\ell - \mathbf{v}^{\ell'}\|_2 \simeq \|\mathbf{y}^\ell - \mathbf{y}^{\ell'}\|_2$$

for all  $\ell, \ell' = 1, \dots, L$ . The latter simplifies as

$$\begin{aligned} \|\mathbf{y}^\ell - \mathbf{y}^{\ell'}\|_2 &= \left\| \begin{bmatrix} \mathbf{K} & \mathbf{L} \\ \mathbf{M} & \mathbf{N} \end{bmatrix} \left( \begin{bmatrix} \mathbf{s}_{\mathcal{M}}^\ell \\ \mathbf{s}_{\mathcal{O}} \end{bmatrix} - \begin{bmatrix} \mathbf{s}_{\mathcal{M}}^{\ell'} \\ \mathbf{s}_{\mathcal{O}} \end{bmatrix} \right) \right\|_2 \\ &= \left\| \begin{bmatrix} \mathbf{K} \\ \mathbf{M} \end{bmatrix} (\mathbf{s}_{\mathcal{M}}^\ell - \mathbf{s}_{\mathcal{M}}^{\ell'}) \right\|_2 \end{aligned}$$

where we have exploited the linearity in (1) together with the fact that non-metered loads remain roughly invariant during probing. We define the distance between  $\mathbf{s}_{\mathcal{M}}^\ell, \mathbf{s}_{\mathcal{M}}^{\ell'} \in \mathcal{S}_r$  as

$$\begin{aligned} d(\ell, \ell') &:= \|\mathbf{y}^\ell - \mathbf{y}^{\ell'}\|_2^2 \\ &= (\mathbf{s}_{\mathcal{M}}^\ell - \mathbf{s}_{\mathcal{M}}^{\ell'})^\top (\mathbf{K}^\top \mathbf{K} + \mathbf{M}^\top \mathbf{M}) (\mathbf{s}_{\mathcal{M}}^\ell - \mathbf{s}_{\mathcal{M}}^{\ell'}). \end{aligned} \quad (9)$$

Based on this metric, we would like to select a subset  $\mathcal{A}$  of  $T$  out of the  $L$  candidate vectors in  $\mathcal{S}_r$  so that the sum of their pairwise distances is maximized

$$\begin{aligned} \max_{\mathcal{A} \subset \mathcal{S}_r} \quad & \sum_{\ell \in \mathcal{A}} \sum_{\ell' \in \mathcal{A}} d(\ell, \ell') \\ \text{s.to} \quad & |\mathcal{A}| = T. \end{aligned} \quad (10)$$

The task in (10) is known as the *max-sum diversity* (MSD) problem, and appears frequently in information retrieval, computational geometry, and operations research [11]. In fact, MSD can be reformulated as a binary quadratic program (QP) after introducing the  $L \times L$  distance matrix  $\mathbf{D}$  with entries  $D_{\ell, \ell'} := d(\ell, \ell')$  as

$$f^* := \max_{\mathbf{x} \in \{0,1\}^L} \mathbf{x}^\top \mathbf{D} \mathbf{x} \quad (11a)$$

$$\text{s.to} \quad \mathbf{x}^\top \mathbf{1} = T. \quad (11b)$$

Despite its simple form, the MSD task is NP-hard [11]. However, thanks to the properties of  $\mathbf{D}$ , the problem in (11) enjoys a polynomial-time approximate scheme (PTAS) [11].

Although  $\mathbf{D}$  is indefinite, the objective in (11a) can be shown to be concave under constraint (11b). To see this, define the  $2N \times L$  matrix  $\tilde{\mathbf{Y}} := [\mathbf{y}_1 \cdots \mathbf{y}_L]$  and use the definition of  $d(\ell, \ell')$  to rewrite the objective of (11) as

$$\begin{aligned} f(\mathbf{x}) &:= \mathbf{x}^\top \mathbf{D} \mathbf{x} = \sum_{\ell=1}^L \sum_{\ell'=1}^L x_\ell x_{\ell'} D_{\ell, \ell'} \\ &= \sum_{\ell=1}^L \sum_{\ell'=1}^L x_\ell x_{\ell'} (\|\mathbf{y}_\ell\|_2^2 + \|\mathbf{y}_{\ell'}\|_2^2 - 2\mathbf{y}_\ell^\top \mathbf{y}_{\ell'}) \\ &= \sum_{\ell'=1}^L x_{\ell'} \|\mathbf{y}_{\ell'}\|_2^2 \left( \sum_{\ell=1}^L x_\ell \right) + \sum_{\ell=1}^L x_\ell \|\mathbf{y}_\ell\|_2^2 \left( \sum_{\ell'=1}^L x_{\ell'} \right) \\ &\quad - 2 \sum_{\ell=1}^L \sum_{\ell'=1}^L x_\ell x_{\ell'} \mathbf{y}_\ell^\top \mathbf{y}_{\ell'} \\ &= 2T \mathbf{c}^\top \mathbf{x} - 2\mathbf{x}^\top \tilde{\mathbf{Y}}^\top \tilde{\mathbf{Y}} \mathbf{x}. \end{aligned}$$

where  $\mathbf{c} := [\|\mathbf{y}_1\|_2^2 \cdots \|\mathbf{y}_L\|_2^2]^\top$ . Since  $\tilde{\mathbf{Y}}^\top \tilde{\mathbf{Y}} \succeq \mathbf{0}$ , the objective  $f(\mathbf{x})$  equals a concave quadratic function.

For moderate  $L$  (a few hundreds), the task in (11) can be handled by a mixed-integer QP solver. For  $T = 2$ , the MSD solution can be found by an exhaustive search. For larger  $T$ , we will use a randomized rounding approach, as adopted from [12] in [11, Remark 2]. The approach is briefly reviewed here for completeness. Its first step solves the relaxed problem

$$\hat{\mathbf{x}} := \arg \min_{\mathbf{0} \leq \mathbf{x} \leq \mathbf{1}} 2\mathbf{x}^\top \tilde{\mathbf{Y}}^\top \tilde{\mathbf{Y}} \mathbf{x} - 2T \mathbf{c}^\top \mathbf{x} \quad (12a)$$

$$\text{s.to} \quad \mathbf{x}^\top \mathbf{1} = T. \quad (12b)$$

Since the binary constraints of (11) are related to box constraints in (12), it holds that  $f(\hat{\mathbf{x}}) \geq f^*$ . To construct a point  $\tilde{\mathbf{x}}$  that is feasible for (11), draw  $L$ -dimensional vectors  $\{\tilde{\mathbf{x}}_i\}$  whose entries are independent Bernoulli random variables with mean  $(1 - \beta)\hat{\mathbf{x}}$  for some  $\beta > 0$ , say  $\beta = 0.1$ . The so constructed binary vectors  $\tilde{\mathbf{x}}_i$ 's satisfy  $\mathbb{E}[\tilde{\mathbf{x}}_i^\top \mathbf{1}] = (1 - \beta)T$  and  $\mathbb{E}[\tilde{\mathbf{x}}_i^\top \mathbf{D} \tilde{\mathbf{x}}_i] = (1 - \beta)^2 \hat{\mathbf{x}}^\top \mathbf{D} \hat{\mathbf{x}}$ . The purpose of scaling  $\hat{\mathbf{x}}$

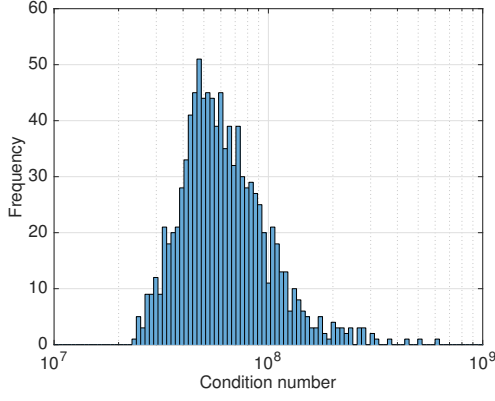


Fig. 2. Histogram of condition numbers for the Jacobian matrix  $\mathbf{J}(\{\mathbf{v}_t\}_{t=1}^4)$  obtained by randomly sampling quadruplets of  $\mathbf{s}_M$ 's from  $\mathcal{S}_r$ .

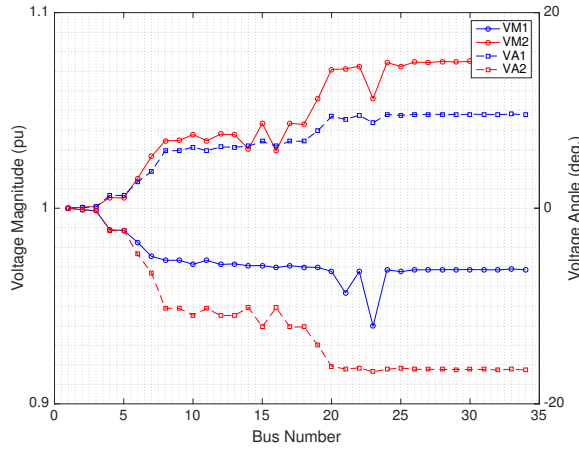


Fig. 3. Probing injection design on the IEEE 34-bus grid for  $T = 2$  and  $O = 6$ . The blue (red) lines correspond to the system states induced by the first (second) probing injection vectors  $\{\mathbf{s}_M^t\}_{t=1}^2$ . Solid lines depict voltage magnitudes, and dashed lines voltage angles.

by  $(1-\beta)$  is to ensure  $\tilde{\mathbf{x}}_i$ 's are both feasible for (11) and yield relatively high cost with significant probability [11].

To justify the need for this third step in probing design, we conducted a test on the IEEE 34-bus feeder for  $T = 4$  and  $O = 6$ . For this test, load uncertainty was confined within a factor of  $\pm 1$  times the nominal loads. Given library  $\mathcal{S}$  of randomized injections drawn from  $\pm 0.2$  pu and obeying (3)–(5), we constructed the reduced library  $\mathcal{S}_r$  based on (8) for  $[\underline{v}, \bar{v}] = [0.90, 1.10]$ . We then solved (12) and followed the randomized rounding process to construct 100 binary  $\tilde{\mathbf{x}}_i$ 's. We evaluated the cost  $f(\tilde{\mathbf{x}}_i)$  for those  $\tilde{\mathbf{x}}_i$ 's satisfying  $\tilde{\mathbf{x}}_i^T \mathbf{1} = T$ , and returned the  $\tilde{\mathbf{x}}_i$  yielding the largest cost. The condition number of the Jacobian matrix evaluated at the so obtained  $\tilde{\mathbf{x}}_i$  was  $3 \cdot 10^6$ . We also calculated the condition number of the Jacobian matrix evaluated at random candidate quadruplets in  $\mathcal{S}_r$ . The latter condition numbers ranged within  $10^7 - 10^9$ ; see Fig. 2. Hence, albeit MSD adds computational complexity, it is an important part of the probing design process.

To show that this MSD step provides diverse system states, we performed another test on the IEEE 34-bus feeder under the same setup, but for  $T = 2$ . The states induced by the designed probing and nominal loads are shown in Figure 3.

Upon solving (10) near optimally, we have obtained  $T$  probing injection vectors  $\{\mathbf{s}_M^t\}_{t=1}^T$  that are implementable by inverters; network-compliant; and yield diverse system states. In the process of probing design, the first step (Section II-A) operates on the entries of  $\mathbf{s}_M^t$ 's; the second step (Section II-B) considers each vector  $\mathbf{s}_M^t$  as a whole; and finally, the third step (Section II-C) accounts for the joint effect of probing injections  $\{\mathbf{s}_M^t\}_{t=1}^T$ .

### III. SOLVING THE P2L TASKS

Recall that the P2L task with phasor data involves solving the set of non-linear equations

$$u_n(\mathbf{v}_t) = u_n^t \quad \forall n \in \mathcal{M}, t \in \mathcal{T} \quad (13a)$$

$$\theta_n(\mathbf{v}_t) = \theta_n^t \quad \forall n \in \mathcal{M}, t \in \mathcal{T} \quad (13b)$$

$$p_n(\mathbf{v}_t) = p_n^t \quad \forall n \in \mathcal{M}, t \in \mathcal{T} \quad (13c)$$

$$q_n(\mathbf{v}_t) = q_n^t \quad \forall n \in \mathcal{M}, t \in \mathcal{T} \quad (13d)$$

$$p_n(\mathbf{v}_t) = p_n(\mathbf{v}_{t+1}) \quad \forall n \in \mathcal{O}, t \in \mathcal{T}' \quad (13e)$$

$$q_n(\mathbf{v}_t) = q_n(\mathbf{v}_{t+1}) \quad \forall n \in \mathcal{O}, t \in \mathcal{T}' \quad (13f)$$

where  $\mathbf{v}_t$ 's are the system states across  $\mathcal{T} = \{1, \dots, T\}$ ;  $\{(u_n^t, \theta_n^t, p_n^t, q_n^t)\}_{n \in \mathcal{M}}$  are the probing data collected at time  $t$ ; (13a)–(13d) are the  $4MT$  metering equations; and (13e)–(13f) are the  $2O(T-1)$  coupling equations with  $\mathcal{T}' := \{1, \dots, T-1\}$ . For the P2L task with non-phasor data, the angle information in (13b) is unavailable.

Having characterized the local identifiability for the P2L tasks in Part I, this section presents solvers for tackling P2L. If grid specifications are noiseless and the power injections in  $\mathcal{O}$  remain unaltered during probing, the P2L tasks boil down to solving the equations in (13). The latter can be tackled by adopting the semidefinite program (SDP)-based solvers developed in [13], [14], [15], [16]. Here we will skip the details, which can be found in [17] for  $T = 2$ , and outline the P2L solver for noisy data.

Probing data are inexact due to measurement noise and modeling inaccuracies in the metering equations of (13a)–(13d). To account for small fluctuations in non-metered loads during probing, a noise term is added to the RHS of the coupling equations in (13e)–(13f). To cope with noisy data, we extend the penalized SDP-based state estimator of [16] to the P2L setting as follows

$$\min \alpha \sum_{t=1}^T \text{Tr}(\mathbf{M}\mathbf{V}_t) + \sum_{t=1}^T \sum_{k=1}^{3M} f_k(\epsilon_k^t) + \sum_{t=1}^{T-1} \sum_{l=1}^{2O} f_l(\xi_l^t) \quad (14a)$$

$$\text{over } \mathbf{V}_t \succeq \mathbf{0}, \{\epsilon_k^t\}_{k=1}^{3M}, t \in \mathcal{T} \quad (14b)$$

$$\{\xi_l^t\}_{l=1}^{2O}, t \in \mathcal{T}' \quad (14c)$$

$$\text{s.to } \text{Tr}(\mathbf{M}_k \mathbf{V}_t) + \epsilon_k^t = \hat{s}_k^t, \quad k = 1 : 3M, t \in \mathcal{T} \quad (14d)$$

$$\text{Tr}(\mathbf{M}_l \mathbf{V}_t) = \text{Tr}(\mathbf{M}_l \mathbf{V}_{t+1}) + \xi_l^t, \quad l = 1 : 2O, t \in \mathcal{T}' \quad (14e)$$

where the given matrices  $\mathbf{M}_k$  depend on  $\mathbf{Y}$ ; see [14], [15].

The matrix variables  $\mathbf{V}_t \succeq \mathbf{0}$  have been obtained upon relaxing the rank-one constraint  $\mathbf{V}_t = \tilde{\mathbf{v}}_t \tilde{\mathbf{v}}_t^H$  on the original system states for  $t \in \mathcal{T}$ . The measurements  $\hat{s}_k^t$  relate to state  $\mathbf{v}_t$  in (14d); and constraint (14e) couples the  $T$  states.

The auxiliary variable  $\epsilon_k^t$  equals the difference between the measurement  $\hat{s}_k^t$  and its noiseless value  $\text{Tr}(\mathbf{M}_k \mathbf{V}_t)$ . This difference is penalized through function  $f_k$  in the objective, and  $f_k$  can be a weighted squared or absolute value, that is

$$f_k(\epsilon_k^t) = \left(\frac{\epsilon_k^t}{\sigma_k}\right)^2 \quad \text{or} \quad f_k(\epsilon_k^t) = \frac{|\epsilon_k^t|}{\sigma_k}$$

with different  $\sigma_k$ 's depending on the uncertainty of the  $k$ -th datum. The optimization variables  $\xi_i^t$ 's capture the deviations of non-metered loads and are penalized through  $f_i$ 's, defined similar to  $f_k$ 's.

The first summand in (14a) corresponds to a regularizer promoting rank-one minimizers for  $\mathbf{V}_t$ ; a practical choice sets  $\mathbf{M} = \mathbf{G}$  as suggested in [15]. The second and third summands in (14a) are data-fitting terms. The tuning parameter  $\alpha > 0$  governs the balance between the regularizer and the data-fitting terms: For  $\alpha = 0$ , the P2L cost involves only the data-fitting terms; whereas for increasing  $\alpha$ , more emphasis is placed on the regularizer [16]. If one or more of the minimizers  $\mathbf{V}_t^*$  of (14) is not rank-one, the heuristic for constructing a system state  $\mathbf{v}_t^*$  proposed in [16] is used.

Additional constraints can be added to strengthen the SDP relaxation. For example, if non-metered buses are known to host exclusively loads, the constraints  $\text{Tr}(\mathbf{M}_l \mathbf{V}_t) \leq 0$  for  $l = 1 : 2O$ , and  $t \in \mathcal{T}$  can be appended to (14). Additional information on loads, such as the uncertainty range of (7), can be readily incorporated. As in [16], if bus  $n$  is known to be a zero-injection bus, then  $\tilde{v}_n = \mathbf{e}_n^\top \mathbf{Y} \tilde{\mathbf{v}}$  has to be zero. Therefore, the constraint  $\tilde{\mathbf{v}}_n^* = \mathbf{V} \mathbf{Y}^* \mathbf{e}_n = \mathbf{0}$  can be added.

Given phasor data, the metering equations corresponding to voltage magnitudes can be dropped. If the vectors of voltage phasors  $\{\tilde{\mathbf{v}}_t\}_{t=1}^T$  are included as optimization variables, the direct measurements on the voltage phasors of  $\mathcal{M}$  can be simply expressed as

$$\tilde{v}_{t,k} + \epsilon_k^t = \hat{s}_k^t, \quad k = 1 : M, \quad t \in \mathcal{T}. \quad (15)$$

To capture the dependence between  $\tilde{\mathbf{v}}_t$  and  $\tilde{\mathbf{V}}_t$ , the non-convex constraint

$$\text{rank} \left( \begin{bmatrix} \mathbf{V}_t & \tilde{\mathbf{v}}_t \\ \tilde{\mathbf{v}}_t^H & 1 \end{bmatrix} \right) = 1$$

can be surrogated by the next SDP constraint as in [13]

$$\begin{bmatrix} \mathbf{V}_t & \tilde{\mathbf{v}}_t \\ \tilde{\mathbf{v}}_t^H & 1 \end{bmatrix} \succeq \mathbf{0}, \quad t \in \mathcal{T}. \quad (16)$$

Since the  $\tilde{\mathbf{v}}_t$ 's are optimization variables now, there is no need to use the heuristic of [16] to recover the system states.

#### IV. NUMERICAL TESTS

The topological observability criteria for the P2L task along with the SDP-based solvers were numerically tested using the IEEE 34-bus feeder. The original multi-phase grid was converted into an equivalent single-phase grid [18]. Ran on a 2.7 GHz Intel Core i5 laptop computer with 8 GB RAM, the P2L tasks were solved within 2-30 sec using the SeDuMi solver in YALMIP and MATLAB [19], [20].

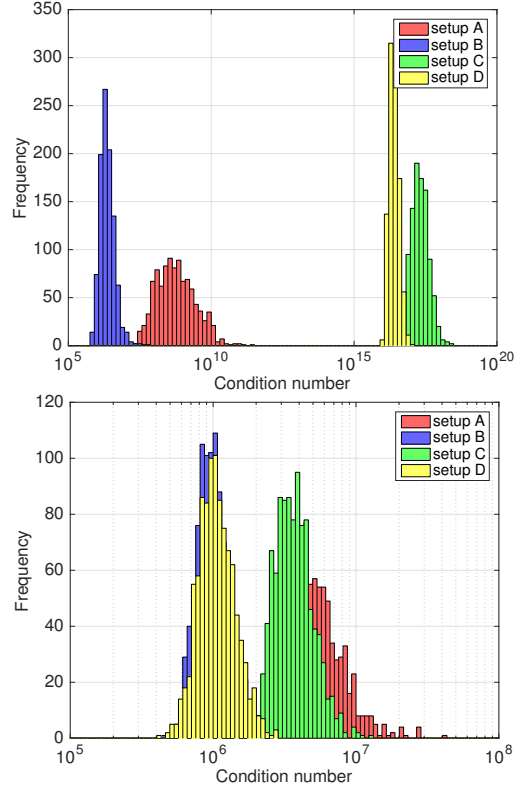


Fig. 4. Histograms of the condition numbers for the P2L Jacobian matrices with non-phasor data for  $T = 2$  (top) and  $T = 4$  (bottom) probing actions.

#### A. Numerical observability

Since Theorems ?? and ?? in Part I rely on the sparsity pattern rather than the exact values of  $\mathbf{J}(\{\mathbf{v}_t\})$ , we evaluated  $\mathbf{J}(\{\mathbf{v}_t\})$  for 1,000 random state sequences  $\{\mathbf{v}_t\}_{t=1}^T$ . The scenarios of non-phasor and phasor probing data were tested under four probing setups. For each probing setup, the location of the non-metered and probing buses were fixed, and 1,000 random state sequences were generated by randomly drawing voltage magnitudes in the range  $[0.90, 1.10]$  pu and voltage angles in the range  $[-15, 15]$  degrees. Assuming non-phasor data first, the following four setups were constructed according to the condition of Th. ?? of Part I:

- Setup A met the condition for  $O = 16$  and  $T = 2$ .
- Setup B met the condition for  $O = 6$  and  $T = 2$ .
- Setup C failed the condition for  $O = 16$  and  $T = 2$ , but met it for  $T = 4$ .
- Setup D failed the condition for  $O = 6$  and  $T = 2$ , but met it for  $T = 4$ .

The same probing setups were considered for phasor data. As discussed in Part I, setups A and B meet also the condition of Th. ?. Additionally, setups C and D were constructed such that they met the condition of Th. ? for  $T = 2$ .

*Non-phasor data:* Figure 4 depicts the condition number histograms obtained under the four setups for  $T = 2$  (top panel) and  $T = 4$  (bottom panel). Under setups A and B, although the dimensions of  $\mathbf{J}(\{\mathbf{v}_t\})$  increase with  $T$ , the condition numbers did not. In fact, the condition number was sometimes reduced, especially in networks with large  $O$ . For

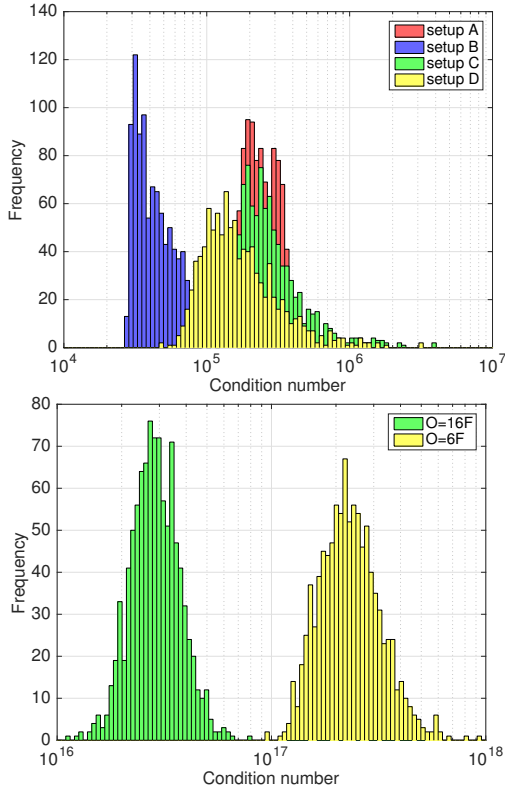


Fig. 5. Histograms of the condition numbers for the P2L Jacobian matrices with phasor data for  $T = 2$  (top) and  $T = 4$  (bottom) probing actions.

setups C and D, there was a significant shift in the histograms from  $T = 2$  to  $T = 4$ , which validates Th. ???. By and large, the condition number improves for decreasing  $O$  and increasing  $T$ . Hence, when more loads are to be recovered, longer probing periods should be used. Of course, longer probing periods may violate the stationarity assumption on loads.

*Phasor data:* Figure 5 displays the condition number histograms of  $\mathbf{J}(\{\mathbf{v}_t\})$  again for  $T = 2$  (top) and  $T = 4$  (bottom). As expected, due to the value added of phasor data, the condition numbers decrease significantly. In addition, setups C and D that failed for  $T = 2$  with non-phasor data, become successful with phasor probing data. The tests corroborate the criteria of Th. ???. The bottom panel of Figure 5 displays the condition number histograms under the following two setups that did not satisfy the condition of Th. ???: *i*) for  $T = 4$  and  $O = 6$  (yellow histogram); and *ii*) for  $T = 4$  and  $O = 16$  (green histogram).

The condition number of the Jacobian matrices in PSSE tasks for transmission systems is known to depend heavily on the specification set [21], [22]: A larger number of voltage magnitude and line flow measurements tends to yield a lower condition number. It is thus expected that adding line flow measurements would improve load and state estimation.

### B. SDP-based P2L

Given noisy specifications, the P2L tasks were tackled using actual data and the SDP-based solver of (14)–(16). The loads

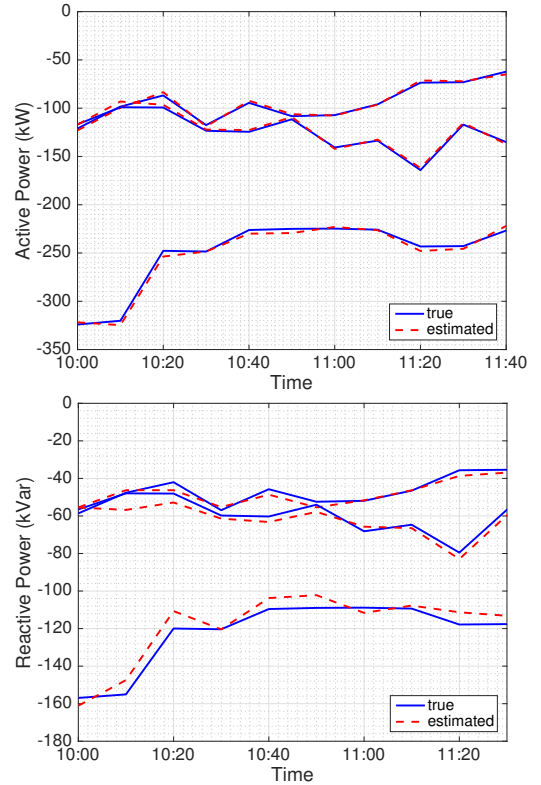


Fig. 6. Active (top) and reactive (bottom) power injection estimates using probing with non-phasor data for  $T = 2$  and  $O = 3$ .

on the IEEE 34-bus grid were taken from the Pecan Street dataset [23], between 10:00 a.m. and 01:40 p.m. on January 1, 2013 and in 10-min intervals. Load sequences were normalized so that active loads lied in the range of  $[0, 0.5]$  pu. Lacking values for reactive loads, a lagging power factor of 0.9 was simulated for all non-metered buses. We first created a data library  $\mathcal{S}$  of 10,000 randomized injection vectors by restricting the inverter apparent power capacity to 0.2 pu. Library  $\mathcal{S}$  was then reduced to  $\mathcal{S}_r$  to ensure that voltage magnitudes lie within  $[0.90, 1.10]$  pu for non-metered loads lying within  $[0, 2s_O]$ , where  $s_O$  consists of the actual non-metered loads. The MSD problem was solved to find the  $T$  most diverse probing injections. For all tests, the regularization parameter was set to  $\alpha = 20,000$  and the functions  $f_k$  and  $f_l$  in (14) were selected as WLS costs with  $\sigma$ 's to be defined shortly.

*Non-phasor data:* The first test compared probing setups for increasing  $T$ . Figures 6 and 7 show the accuracy in estimating the non-metered loads on buses  $\{4, 15, 16\}$  for  $T = 2$  and  $T = 6$ , respectively. The measurement noise was modeled as zero-mean Gaussian with standard deviation of  $1.5 \cdot 10^{-4}$  times the corresponding noiseless values of squared voltage magnitudes and nodal active/reactive powers. Lacking sub-minute load data, the noise on non-metered buses was modeled similarly. Figures 6 and 7 show that load estimation accuracy improves with increasing  $T$ . This can be attributed to a lower condition number of the associated Jacobian  $\mathbf{J}(\{\mathbf{v}_t\})$ . To corroborate Th. ?? in Part I, we also conducted numerical tests on meshed networks and obtained similar results. Having access to phasor measurements is only expected to increase the

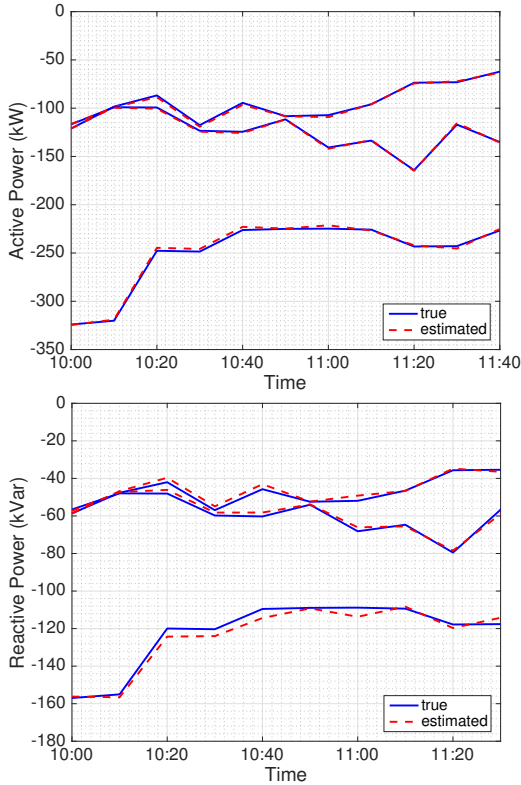


Fig. 7. Active (top) and reactive (bottom) power injection estimates using probing with non-phasor data for  $T = 6$  and  $O = 3$ .

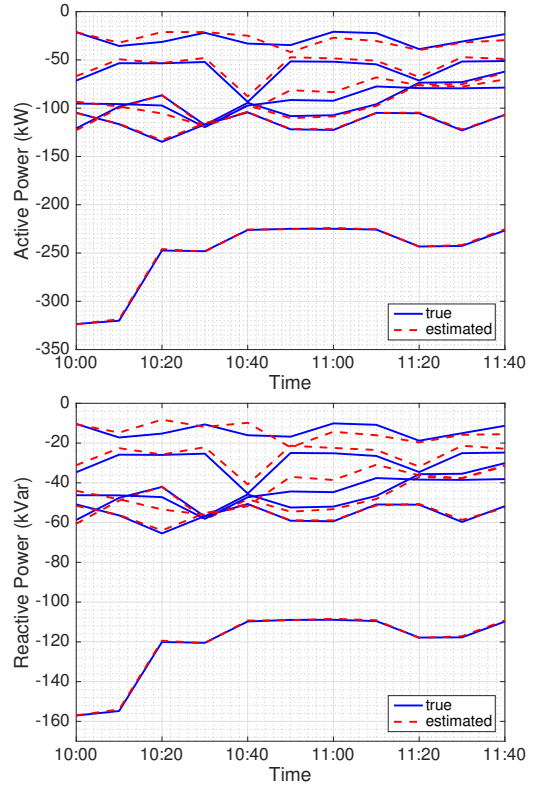


Fig. 8. Active (top) and reactive (bottom) power injection estimates using probing with phasor data for  $T = 4$  and  $O = 6$ .

estimation accuracy; some results are provided next.

*Phasor data:* Figures 8 and 9 present the accuracy in estimating the non-metered loads on buses  $\{4, 6, 15, 20, 27, 31\}$  respectively for  $T = 4$  and  $T = 6$ . The measurement noise was modeled as before, while the noise on non-metered buses was modeled zero-mean Gaussian with standard deviation of 0.001 times the related noiseless values.

To push the limits of the P2L scheme in recovering non-metered loads, complex voltage measurements from metered nodes were assumed noiseless, while the noise on (re)active injections and load variations was simulated as zero-mean Gaussian with standard deviation of 0.01 times the associated noiseless values. To corroborate the applicability of Th. ?? to meshed networks, this test was ran on a modified IEEE 34-bus feeder with two extra branches connecting buses  $(2, 23)$  and  $(7, 32)$ . Figure 10 shows the superior estimates of non-metered loads on buses  $\{2, 4, 6, 8, 15, 16, 20, 23, 27, 33\}$  with just two probing actions. Clearly, having low-noise readings of voltage phasors is crucial in recovering loads. The estimates of Figure 10 are relatively precise, even though injection measurements exhibit larger noise and the stationarity assumption of the non-metered loads is violated. Although the previous tests assumed measurements with smaller noise, such quality of measurements is expected from high-accuracy smart meters or PMUs [24]. Several tests were also conducted with measurements corrupted by high-variance noise. While it was not possible to accurately recover loads under such regimes, the solver was still able to find a reasonably good estimate of the system state.

## V. CONCLUSIONS

The novel data acquisition scheme of probing an electric grid via smart inverters to infer non-metered loads has been presented. Part I studied the topological observability of grid probing using (non)-phasor data in potentially meshed networks. If a probing setup is deemed topologically observable, Part II has presented a systematic methodology for designing probing injections. The goal is improved estimation accuracy and adherence to inverter and feeder constraints even without knowing non-metered loads. The computational tasks involved in grid probing have been cast as penalized SDP-based solvers and account for noisy measurements and non-stationary loads.

Numerical tests using synthetic and real-world data on benchmark feeders demonstrate the ensuing take-away simulation findings: *i)* High-accuracy phasor data are better for load recovery than non-phasor data; *ii)* Having the most diverse system states during probing yields better load estimates; *iii)* Probing seemed to yield better estimates under broad voltage regulation range and tight load uncertainty *iv)* Although increasing  $T$  improved the system state accuracy, the obtained load estimates were not always better, especially for larger  $O$ . Nevertheless, we were able to recover a reasonable number of loads; and *v)* Including the extra constraints to strengthen the SDP relaxation provided better numerical accuracy.

Several questions remain open. Generalizing probing to infer the parameters of ZIP loads; developing scalable solvers perhaps along the lines of [3]; incorporating measurement from distribution lines and transformers [25]; and applying our topological observability framework to detect data attacks in

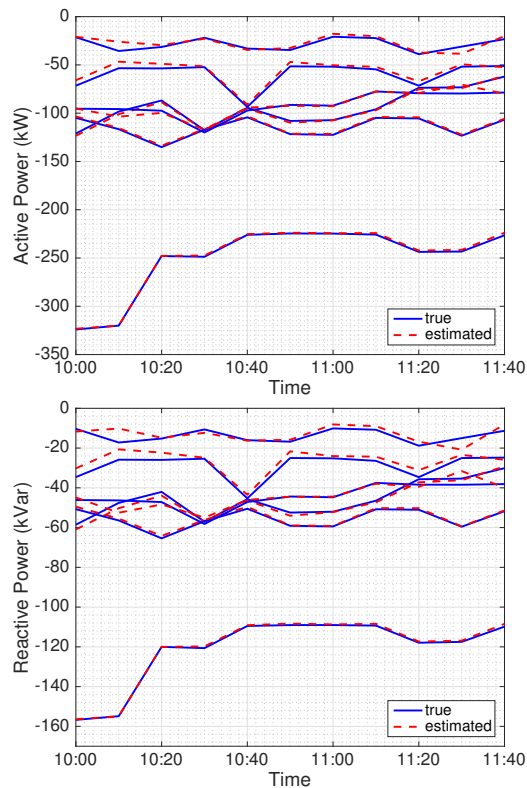


Fig. 9. Active (top) and reactive (bottom) power injection estimates using probing with phasor data for  $T = 6$  and  $O = 6$ .

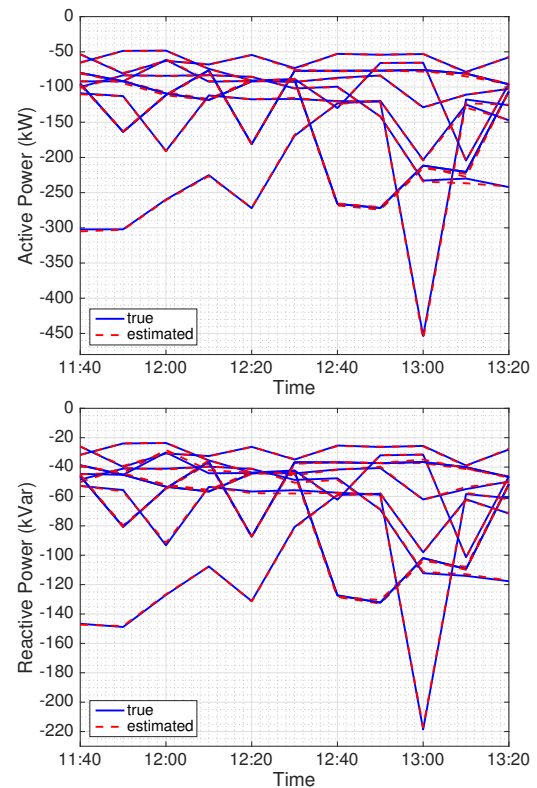


Fig. 10. Active (top) and reactive (bottom) power injection estimates using probing with phasor data for  $T = 2$  and  $O = 10$ .

distribution grids; all constitute pertinent research directions.

## REFERENCES

- [1] A. Gómez-Expósito, A. J. Conejo, and C. Canizares, Eds., *Electric Energy Systems, Analysis and Operation*. Boca Raton, FL: CRC Press, 2009.
- [2] Y. Weng, R. Rajagopal, and B. Zhang, “Geometric understanding of the stability of power flow solutions,” 2017. [Online]. Available: <https://arxiv.org/abs/1706.07401>
- [3] G. Wang, A. S. Zamzam, G. B. Giannakis, and N. D. Sidiropoulos, “Power system state estimation via feasible point pursuit: Algorithms and Cramer-Rao bound,” *IEEE Trans. Signal Processing*, vol. 66, no. 6, pp. 1649–1658, Mar. 2018.
- [4] S. Bolognani and F. Dorfler, “Fast power system analysis via implicit linearization of the power flow manifold,” in *Proc. Allerton Conf. on Comm., Control, and Computing*, Allerton, IL, Sep. 2015, pp. 402–409.
- [5] D. Deka, M. Chertkov, and S. Backhaus, “Structure learning in power distribution networks,” *IEEE Trans. Control of Network Systems*, pp. 1–1, 2017, (early access).
- [6] M. Baran and F. Wu, “Optimal sizing of capacitors placed on a radial distribution system,” *IEEE Trans. Power Syst.*, vol. 4, no. 1, pp. 735–743, Jan. 1989.
- [7] G. Cavraro, V. Kekatos, and S. Veeramachaneni, “Voltage analytics for power distribution network topology verification,” *IEEE Trans. Smart Grid*, pp. 1–1, (early access) 2017.
- [8] B. C. Eaves and R. M. Freund, “Optimal scaling of balls and polyhedra,” *Mathematical Programming*, vol. 23, no. 1, pp. 138–147, Dec. 1982.
- [9] O. Mangasarian, “Set containment characterization,” *Journal of Global Optimization*, vol. 24, no. 4, pp. 473–480, Dec. 2002.
- [10] L. Zhao, W. Zhang, H. Hao, and K. Kalsi, “A geometric approach to aggregate flexibility modeling of thermostatically controlled loads,” *IEEE Trans. Power Syst.*, vol. 32, no. 6, pp. 4721–4731, Nov. 2017.
- [11] A. Cevallos, F. Eisenbrand, and R. Zenklusen, “Max-sum diversity via convex programming,” in *Intl. Symp. on Comp. Geometry*, vol. 51, no. 26, Dagstuhl, Germany, 2016, pp. 1–14.
- [12] P. Raghavan and C. D. Tompson, “Randomized rounding: A technique for provably good algorithms and algorithmic proofs,” *Combinatorica*, vol. 7, no. 4, pp. 365–374, Dec. 1987.
- [13] H. Zhu and G. B. Giannakis, “Power system nonlinear state estimation using distributed semidefinite programming,” *IEEE J. Sel. Topics Signal Process.*, vol. 8, no. 6, pp. 1039–1050, Dec. 2014.
- [14] C. Klauber and H. Zhu, “Distribution system state estimation using semidefinite programming,” in *Proc. North American Power Symposium*, Charlotte, NC, Oct. 2015.
- [15] R. Madani, J. Lavaei, and R. Baldick, “Convexification of power flow problem over arbitrary networks,” in *Proc. IEEE Conf. on Decision and Control*, Osaka, Japan, Dec. 2015.
- [16] R. Madani, A. Ashraphijuo, J. Lavaei, and R. Baldick, “Power system state estimation with a limited number of measurements,” in *Proc. IEEE Conf. on Decision and Control*, Las Vegas, NV, Dec. 2016.
- [17] S. Bhela, V. Kekatos, and S. Veeramachaneni, “Enhancing observability in distribution grids using smart meter data,” *IEEE Trans. Smart Grid*, vol. PP, no. 99, pp. 1–9, 2017.
- [18] L. Gan, N. Li, U. Topcu, and S. Low, “On the exactness of convex relaxation for optimal power flow in tree networks,” in *Proc. IEEE Conf. on Decision and Control*, Maui, HI, Dec. 2012, pp. 465–471.
- [19] J. Lofberg, “A toolbox for modeling and optimization in MATLAB,” in *Proc. of the CACSD Conf.*, 2004. [Online]. Available: <http://users.isy.liu.se/johan/yalmp/>
- [20] J. F. Sturm, “Using SeDuMi 1.02, a Matlab toolbox for optimization over symmetric cones,” *Optimization Methods Software*, vol. 11–12, pp. 625–653, Aug. 1999. [Online]. Available: <http://sedumi.ie.lehigh.edu>
- [21] J. W. Gu, K. A. Clements, G. R. Krumpholz, and P. W. Davis, “The solution of ill-conditioned power system state estimation problems via the method of peters and wilkinson,” *IEEE Trans. Power App. Syst.*, vol. PAS-102, no. 10, pp. 3473–3480, Oct. 1983.
- [22] R. Ebrahimian and R. Baldick, “State estimator condition number analysis,” *IEEE Trans. Power Syst.*, vol. 16, no. 2, pp. 273–279, May 2001.
- [23] (2013) Pecan Street Inc. [Online]. Available: [dataport.pecanstreet.org/](http://dataport.pecanstreet.org/)
- [24] G. Frigo, C. Narduzzi, D. Colangelo, M. Pignati, and M. Paolone, “Definition and assessment of reference values for PMU calibration in static and transient conditions,” in *IEEE Intl. Workshop on Applied Measurements for Power Systems*, Aachen, Germany, Sep. 2016.
- [25] R. Sevljan and R. Rajagopal, “Distribution system topology detection using consumer load and line flow measurements,” 2015. [Online]. Available: <http://arxiv.org/abs/1503.07224>